# Electron-impact ionization of W⁵⁺

V. Jonauskas ◉,[1,*] A. Kynienė,[1] S. Kučas,[1] S. Pakalka,[1] Š. Masys,[1] A. Prancikevičius,[2] A. Borovik Jr.,[3,†]
M. F. Gharaibeh,[4] S. Schippers,[3] and A. Müller[5]

[1]*Institute of Theoretical Physics and Astronomy, Vilnius University, Saulėtekio alėja 3, LT-10257 Vilnius, Lithuania*
[2]*Leiden Institute of Physics, Leiden University, P.O. Box 9504, 2300 RA Leiden, The Netherlands*
[3]*I. Physikalisches Institut, Justus-Liebig-Universität Gießen, Heinrich-Buff-Ring 16, D-35392 Giessen, Germany*
[4]*College of Arts and Sciences, Department of Mathematics, Statistics and Physics, Qatar University, P.O. Box 2713, Doha, Qatar*
[5]*Institut für Atom- und Molekülphysik, Justus-Liebig-Universität Gießen, Leihgesterner Weg 217, D-35392 Giessen, Germany*

Electron-impact single-ionization cross sections for the W⁵⁺ ion have been studied experimentally and theoretically. Measurements of a detailed ionization spectrum and of absolute cross sections were performed employing the crossed-beams method in the energy range from the ionization onset up to 1000 eV. The experimental data show a prominent contribution of W⁵⁺ ions in metastable states. The theoretical analysis includes level-to-level calculations from the $4f^{14}5s^25p^65d$ ground configuration and long-lived levels of the $6s$, $5p^55d^2$, $4f^{13}5d^2$, and $4f^{13}5d\,6s$ configurations. Direct-ionization and excitation-autoionization contributions to the total single-ionization cross sections were calculated employing a distorted-wave approximation. Radiative damping was taken into account. It is shown that correlation effects play an important role and lead to substantial reduction of cross sections. Theory and experiment are in quite good agreement when, within a statistical model, a $(85 \pm 9)\%$ fraction of parent ions in the ground configuration is assumed. The strongest contributions of metastable parent ions arise from the $5p^55d^2$ and $4f^{13}5d^2$ configurations.

## I. INTRODUCTION

Tungsten is used to cover parts of the inner walls in current and future fusion devices. Bombardment of the walls with energetic particles leads to ejection of tungsten atoms which can drift into the central regions of the thermonuclear plasma. On their way from the wall region to the plasma center, tungsten atoms are ionized many times. Depending on the plasma temperature only few electrons can remain bound to the tungsten nucleus. Electron-impact single ionization is the strongest among all ionization processes. Therefore, fusion-plasma modeling requires the knowledge of ionization cross sections for tungsten ions up to the highest charge states.

The first experimental cross sections for single ionization of W⁺ were presented by Montague and Harrison [1]. The data favorably compared with the later measurements by Stenke *et al.* [2] covering the range of W$^{q+}$ ions with $q = 1, ..., 10$. Additional experimental cross sections were published for W¹⁷⁺ [3] and W¹⁹⁺ [4]. The remaining gap of low to moderately high charge states was recently filled by measurements for W$^{q+}$ ions with $q = 11–16, 18$ [5]. Multiple ionization of tungsten ions by electron impact has also been investigated for several charge states [3,6]. All of these experiments were carried out with charge-purified and mostly also isotopically-cleaned tungsten ion beams. However, the initial electronic states of the ions, particularly for $q > 1$, could not be equally well defined. The ions were generated in an ion-source plasma that populated excited states according to the plasma temperature. As a result, the cross sections measured in interacting-beams experiments are typically not for the ground state of the investigated ion but for a mixture of ions in different long-lived electronic levels. In a fusion plasma the ions in a given charge state associated with a certain plasma temperature are likely to be in similar states of excitation so that the measured cross sections provide suitable information for fusion-plasma modeling. Among all the tungsten ions investigated so far in ionization experiments, the W⁵⁺ ion features the most prominent cross-section signature of the presence of metastable excited states. For the clarification of this signature, manifesting itself by the occurrence of ionization signal at energies well below the ground-state ionization threshold, the present investigation was initiated.

Stenke *et al.* [2] compared their measurements with the semiempirical Lotz formula [7], which provides electron-impact direct single-ionization cross sections (while neglecting contributions of excitation with subsequent autoionization). The ionization potentials and the numbers of electrons in each subshell are used in the Lotz formula as parameters. The calculated cross sections are approximately 40% below the experimental data for the peak values which is caused by the missing contributions from indirect ionization processes. The Lotz formula is based on scaling behavior of electron-impact direct single ionization of atoms and ions. Scaling properties and the deduction of universal cross-section shape functions for the ionization of atomic targets can be used to predict cross sections for electron-impact single or even multiple ionization. Scaling rules have been discussed by Aichele *et al.* [8] in connection with ionization of

---

*valdas.jonauskas@tfai.vu.lt
†alexander.borovik@physik.uni-giessen.de

hydrogenlike ions. Their application of the analytical parametrization of the shape of atomic ionization cross sections proposed by Rost and Pattard [9] shows excellent agreement with the available experimental data. Ancarani and Hervieux [10] developed a scaling law and successfully applied it to electron-impact ionization cross sections of Li-like ions. A new ionization scaling law was found by Szłuińska *et al.* [11] and was applied to neutral atoms along columns of the periodic table. The most recent treatments of electron-impact single-ionization scaling behavior were published by Bray *et al.* [12] and de Avillez *et al.* [13].

Similarly, numerous attempts have been made to find suitable scaling rules for multiple ionization of atoms and ions by electron impact. Rost and Pattard [14] derived a universal shape function for the electron-impact double ionization of negative ions and demonstrated its validity by comparison with experimental results of Defrance's group [15,16]. Complex multielectron ions were investigated for example by Aichele *et al.* [17] who measured single- and multiple-ionization cross sections for several charge states of praseodymium ions and compared their results with scaling rules developed by Bélenger *et al.* [18] and Fisher *et al.* [19]. A recent comprehensive overview of multiple ionization by electron impact and the application of scaling formulas has been provided for atoms and ions of He through Zn [20]. None of the proposed scaling rules can presently claim to provide reliable cross-section data for electron-impact single and multiple ionization of tungsten atoms or ions except maybe for the highest charge states. Advanced theoretical calculations are necessary to provide data where there are no experiments.

A theoretical study of electron-impact single ionization of $W^{5+}$ ions from the ground configuration using the configuration-average distorted-wave (CADW) approach [21] showed good agreement with the experiment at electron energies $E_e$ above the single-ionization threshold up to 500 eV. However, there are two weak points in that calculation. First, the configuration-average approach produces unreliable results for configurations whose levels straddle the ionization threshold. Second, the experimentally observed $W^{5+}$ cross-section onset which originates from the presence of metastable ions in the parent ion beam was not quantitatively considered. The same is true for the other theoretical calculations of electron-impact single-ionization cross sections for the $W^{5+}$ ion and their comparison with experiment. Loch *et al.* [22] reported ionization cross-section calculations for tungsten atoms in all charge states $q$ up to 73 but provided data only for the charge states $q = 9, 22, 45, 63, 64,$ and 72. The CADW approach was also applied to the investigation of ionization processes in the neutral W atom [23]. Demura *et al.* [24] employed a statistical model based on the idea of collective excitations of atomic electrons with the local plasma frequency and the Thomas-Fermi model is used to describe atomic electron-density distributions. While this approach may be successfully used for a first estimate of cross sections over a wide range of targets it does not reproduce details of experimental data. More recently, Zhang *et al.* [25] carried out detailed level-to-level distorted-wave (LLDW) calculations but, like all other theory groups before, did not consider contributions arising from $W^{5+}$ parent ions in metastable

levels. More importantly, they realized that the inclusion of excitations to higher shells ($n > 8$) led to overestimated cross sections compared to the measurements. The reason of the discrepancy between the more complete theoretical and the existing experimental values was not identified [25]. It should be noted that the binary-encounter Bethe (BEB) model was used previously to calculate electron-impact cross sections for the neutral W atom and the $W^+$ ion [26] since DW calculations overestimate electron-impact ionization of neutral atoms and near-neutral ions. Later, the same ion species were investigated using the Coulomb-Born method with exchange and normalization [27]. LLDW calculations of cross sections for the $W^+$ ion were also performed by Kwon *et al.* [28] employing the flexible atomic code (FAC) [29]. The excitation of $W^{3+}$ leading to autoionization in addition to the direct-ionization processes was studied using an R-matrix method [30].

In the present work, we calculate and reproduce the complete experimental single-ionization cross-section function for $W^{5+}$ which was measured with a primary ion beam containing ions in long-lived excited levels. In addition, we quantify the metastable fraction of ions in the parent beam. For the $W^{5+}$ ion, a significant ionization onset was found at about 30 eV. It was suggested to be due to the ionization of $5p^5 5d^2$ and $4f^{13} 5d^2$ configurations via excitation-autoionization (EA) processes [2]. Conclusions were based on the analysis of the ionization threshold energies of these configurations. It was further suggested that the direct-ionization (DI) threshold energies of the $5p^5 5d^2$ and $4f^{13} 5d^2$ configurations are similar to the ones of the $4f^{14} 5s^2 5p^6 5d$ ground configuration.

The main goal of the current work is to present detailed experimental electron-impact single ionization cross sections of the $W^{5+}$ ion as well as their comprehensive theoretical analysis. The theoretical study includes direct and indirect processes. Level-to-level calculations were performed for the $5d$ ground configuration and for several excited configurations of $W^{5+}$. For all contributions considered in the determination of the total single-ionization cross section, autoionization branching ratios for every level of the $W^{5+}$ ion populated by excitation of one of the initial states were calculated accounting for Auger and radiative decays from the level. Moreover, the effect of configuration interactions on the cross sections was carefully studied.

The remainder of this paper is organized as follows. In Sec. II, we present the experimental method used to obtain absolute single-ionization cross sections and a detailed ionization spectrum for which the electron energy was scanned in steps of only about 0.2 eV. In Sec. III, we describe the theoretical methods employed for calculating the atomic structure and we present the scattering calculations that were undertaken to determine total ionization cross sections for the $W^{5+}$ ion. In Sec. IV, the obtained results are discussed.

## II. EXPERIMENT

Measurements of the electron-impact single-ionization cross section of $W^{5+}$ ions have been performed at the electron-ion crossed-beams setup, which has been successfully used for cross-section studies of a wide range of ions (see Ref. [31] and references therein). Absolute cross sections

were measured using the well-established animated-beams technique [32–34]. In addition, a high-resolution energy-scan technique was used to uncover fine details in the energy dependence of the measured cross sections [35–37]. Detailed descriptions of the apparatus have been provided previously [38,39] and the details of the experimental procedures were recently discussed by Borovik Jr. *et al.* [40] and Rausch *et al.* [3]. Therefore, only a brief overview of the measurements and the experimental conditions is given here.

Fivefold-charged tungsten ions were produced in a 10 GHz all-permanent-magnet electron-cyclotron-resonance (ECR) ion source [41]. A mixture of ions including all atoms, molecules or clusters present in the source plasma with their specific isotope abundances and their different charge states was extracted from the ECR plasma and accelerated by a voltage of 12 kV. A typical mass spectrum has been provided in a previous review article [42]. The desired $^{186}$W$^{5+}$ ions were selected by properly setting the field of a dipole analyzing magnet. The selected isotopically clean $^{186}$W$^{5+}$ ion beam was charge-state purified once again by a 90° electrostatic deflector and thereby directed into the electron-ion collision region. Two sets of four-jaw slits separated by about 18 cm from one another served for collimation of the ion beam in front of the interaction region where the primary ion beam was crossed by an intense ribbon-shaped electron beam [43]. For the measurements of absolute cross sections the primary ion beam was collimated to a size of only $0.5 \times 0.5$ mm$^2$ to ensure the complete transmission of both the parent ion beam to the Faraday cup and the product ions to the detector during all phases of the experiment while the ion beam crossed different regions of the moving electron gun. Typical beam currents were 4.8 nA under these conditions. For the fine-step scan measurements, the collimation conditions could be relaxed because the electron gun was kept at a fixed position with optimum overlap of the electron and ion beams. The ion beam size was increased to $1.0 \times 1.0$ mm$^2$ resulting in a typical W$^{5+}$ ion current of 6.4 nA. Ionic electron-ion collision products and the primary ion beam were separated by a second dipole magnet, identical to the first one. The ionized ions were registered by a single-particle detector [44,45] after passing an electrostatic out-of-plane 180° spherical deflector. The primary ion beam was collected in a movable Faraday cup appropriately positioned inside the chamber of the second magnet. The signal-to-background ratio at the cross section maximum was approximately 23.

The systematic uncertainty of the absolute cross-section determination [33] is obtained as the quadrature sum of the systematic uncertainties of the parameters entering the cross-section evaluation and equaled 6.3%. An energy-dependent uncertainty due to the limited knowledge of electron-beam transmission through the interaction region, which amounts to 10% at 20 eV and less than 1% at electron energies beyond 120 eV, was also considered. Details considering the cross-section determination procedure, as well as the required parameters and their contributions have been discussed previously [3]. The statistical uncertainties of the absolute cross-section values do not exceed 1% at energies above the threshold for ionization from the ground state. The resulting total uncertainties of the present cross sections have been determined from the square root of the sum of squared individual

systematic uncertainties listed above including the squared statistical uncertainty. Resulting total error bars vary from 11% at 37 eV through 7.9% at 1000 eV at a confidence level of 95%. The energy scale of the cross section measurements is estimated to have an uncertainty of less than ±1 eV. It has been corrected for possible contact-potential effects by comparison of the measured and expected ionization thresholds of He$^+$ ions.

## III. THEORETICAL METHODS

The flexible atomic code [29], which employs the Dirac-Fock-Slater method, is used to calculate energy levels, Auger transition probabilities, and electron-impact excitation and ionization cross sections. The code implements the $jj$-coupling scheme. The cross sections are obtained in the distorted wave (DW) approximation. Previous studies have confirmed the utility of DW calculations for atomic scattering problems like the present one [21,22,46,47]. The local central potentials for the ground configurations of every ion are used to generate the necessary bound and continuum wave functions for each ion.

Direct and indirect processes are investigated to obtain electron-impact single-ionization cross sections from level $i$ of the W$^{5+}$ ion to level $j$ of W$^{6+}$:

$$\sigma_{ij}(E_e) = \sigma_{ij}^{DI}(E_e) + \sum_k \sigma_{ik}^{\text{exc}}(E_e)B_{kj}, \qquad (1)$$

where $\sigma_{ij}^{DI}(E_e)$ is the DI cross section at electron energy $E_e$, $\sigma_{ik}^{\text{exc}}$ is the electron-impact excitation cross section, and the branching ratio is defined by the expression:

$$B_{kj} = \frac{A_{kj}^a + \sum_n A_{kn}^r B_{nj}}{\sum_m A_{km}^a + \sum_n A_{kn}^r}. \qquad (2)$$

$A_{kj}^a$ and $A_{kn}^r$ are Auger and radiative transition probabilities, respectively. The second term in the numerator represents the decay to the final level $j$ through intermediate levels $n$ reached by a radiative transition from the initial excited level $k$. This higher-order term is not included in the current calculations. Its full treatment would drastically increase the computational effort. The total ionization cross section is obtained by summing over all final levels in Eq. (1). The inclusion of the branching ratios in the cross-section calculation automatically takes care of radiative damping of the EA processes.

Excitations of the $4f$, $5s$, $5p$, and $5d$ electrons from the $5d$, $6s$, $4f^{13}5d^2$, $5p^55d^2$, and $4f^{13}5d\,6s$ configurations up to the shells with $n = 12$ are taken into account in the study to ensure convergence of the EA data. Furthermore, the excitations to all subshells with orbital quantum numbers $l \leqslant 6$ are studied and accounted for in the determination of cross sections.

The influence of initial- and final-state correlation on electron-impact ionization cross sections from the ground configuration is investigated. Correlation is taken care of by the implementation of configuration interaction applying suitable basis sets. The correlation effects are studied for the strongest DI channels and excitations that lead to single ionization. The methodology of configuration interaction strength (CIS) is employed to determine a list of admixed configurations having the largest influence on the configuration

under consideration. The CIS was defined previously by the following equation [48,49]:

$$T(K, K') = \frac{\sum_{\gamma\gamma'}\langle\Phi(K\gamma)|H|\Phi(K'\gamma')\rangle^2}{\bar{E}(K, K')^2}. \tag{3}$$

This quantity divided by the statistical weight $g(K)$ of the studied configuration $K$ has the meaning of the average con-

tribution of the admixed configuration $K'$ to the expansion of the wave function for $K$. The summation in Eq. (3) is performed over all states $\gamma$ and $\gamma'$ of the $K$ and $K'$ configurations, respectively. The quantity $\langle\Phi(K\gamma)|H|\Phi(K'\gamma')\rangle$ is the interconfiguration matrix element of the two-electron electrostatic Hamiltonian and $\bar{E}(K, K')$ is an average energy difference between the configurations:

$$\bar{E}(K, K') = \frac{\sum_{\gamma\gamma'}[\langle\Phi(K\gamma)|H|\Phi(K\gamma)\rangle - \langle\Phi(K'\gamma')|H|\Phi(K'\gamma')\rangle]\langle\Phi(K\gamma)|H|\Phi(K'\gamma')\rangle^2}{\sum_{\gamma\gamma'}\langle\Phi(K\gamma)|H|\Phi(K'\gamma')\rangle^2}. \tag{4}$$

The list of admixed configurations is built by considering single and double excitations from all shells with principal quantum numbers $3 \leqslant n \leqslant 8$. The pseudorelativistic method [50] is used to obtain radial orbitals for the studied configurations.

The experimental data show obvious signatures of the presence of ions in long-lived excited states in the primary $W^{5+}$ ion beam employed for the measurements. Therefore, electron-impact excitation and ionization cross sections are calculated both from the levels of the ground electron configuration and from the long-lived levels of the excited $6s$, $4f^{13}5d^2$, $5p^55d^2$, and $4f^{13}5d\,6s$ configurations. Since the experiment did not directly provide information about the relative fractions of ions in certain electronic levels an attempt has to be made to model the experimental cross-section function $\sigma^{\exp}(E_e)$ by a linear combination of the theoretical cross sections $\sigma_i^{\mathrm{th}}(E_e)$ calculated for ions in initial levels $i$. The fractions $\lambda_i$ (with $\sum\lambda_i = 1$) by which the levels $i$ contribute to the model cross section are to be determined by comparison of the weighted sum of the theoretical cross sections with the experimental data. Ideally, the experimental cross section can be expressed by

$$\sigma^{\exp}(E_e) = \sum_{i=1}^{m}\lambda_i\sigma_i^{\mathrm{th}}(E_e), \tag{5}$$

with a suitable set of ion-beam fractions $\lambda_i$. Here, $m$ is the number of levels contributing to the measurements.

## IV. RESULTS

### A. Energy levels

Level energies for the energetically lowest configurations as well as for configurations produced by the strongest excitations from the ground configuration of the $W^{5+}$ ion are presented in Fig. 1. In addition, configurations of $W^{6+}$ ions produced by collisional single ionization of $W^{5+}$ to levels below the double-ionization threshold are shown. Moreover, the energetically lowest levels in $W^{7+}$ that can be reached from $W^{5+}$ by direct double ionization are indicated.

Figure 1 clearly shows that energy levels of the $5p^55d6p$ configurations straddle the ground level of the $W^{6+}$ ion. In addition, the $5p^55d\,6s$ configuration (not shown in the figure) has energy levels above and below the ionization threshold. Contributions from these autoionizing configurations to the

total single-ionization cross sections using the configuration-averaged approach can easily provide inaccurate results. Level-to-level calculations are needed in these cases. It should be noted that DI from the $4d$ subshell in $W^{5+}$ only contributes to indirect processes that end up in net double ionization because the energy levels of the $4d^95d$ configuration are above the ionization threshold of the $W^{6+}$ ion. Levels in the $4d^95d$ configuration can decay via radiative and Auger transitions. However, the fluorescence yields calculated in the single-configuration approximation do not exceed $2 \times 10^{-4}$ for those levels which, therefore, primarily produce the final charge state $W^{7+}$.

### B. Comparison of theoretical and experimental cross sections

The present experimental electron-impact single-ionization cross sections of $W^{5+}$ are shown in Fig. 2 and compared to the previous measurements of Stenke *et al.* [2]. Both data sets have the same trend: the cross section is non-zero at energies well below the ground-state ionization threshold (64.77 eV [51] marked by the vertical arrow). A first onset can be discerned at an electron energy slightly above 20 eV. A rapid increase is observed between about 30 and 35 eV followed by a plateau which extends to energies up to approximately 60 to 70 eV. This part of the cross section
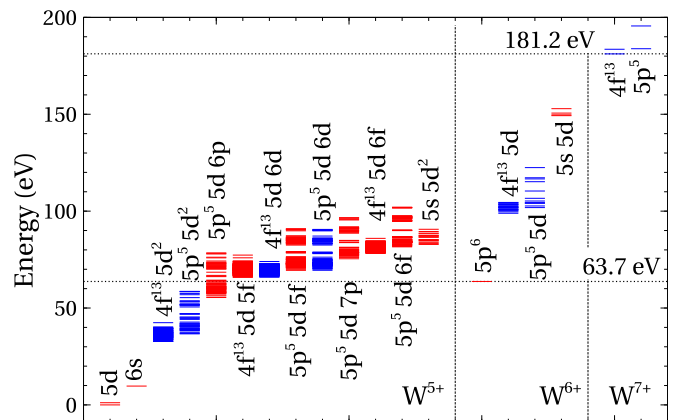


FIG. 1. Energy levels of the main configurations of $W^{5+}$, $W^{6+}$, and $W^{7+}$ ions relevant for the present study. Even configurations are shown in red, odd configurations in blue. Dotted horizontal lines mark the thresholds for single and double ionization of $W^{5+}$, respectively.
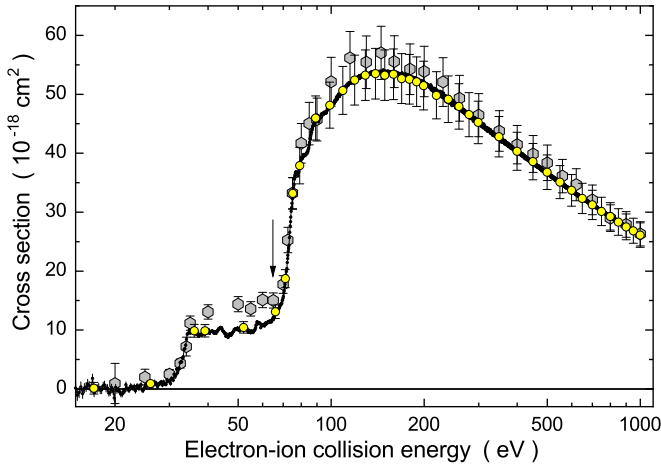
FIG. 2. Present experimental electron-impact ionization cross section of W$^{5+}$ ions (circles with (yellow) shading with total error bars: absolute cross sections; black dots with statistical error bars: results of the fine-step energy scan normalized to the absolute data points) compared to the previous measurements presented by Stenke *et al.* [2] (gray-shaded hexagons with total error bars). The vertical arrow marks the position of the threshold for ionization from the $5d\,^2D_{3/2}$ ground level [51].

clearly indicates the presence of excited ion-beam admixtures in both the present and the previous experiments. At the same time, the heights of the plateaus in these two data sets are different: the cross sections measured by Stenke *et al.* [2] are about 30% higher than the present data. The reason for this, most probably, is in the different amounts of excited ion-beam admixtures produced with two different types of ECR ion sources employed in the different experiments. The main cross-section onset is observed beyond the ground-state ionization threshold. From here on and up to 750 eV, both data sets agree within their error bars. Beyond 750 eV and up to 1000 eV, the two data sets perfectly agree with one another. In addition to absolute cross sections, the present data include the result of a fine-step energy scan which shows clearly distinguishable structures. Step-like features in the measured cross section at energies below 100 eV are invoked by indirect ionization processes involving excitation of inner subshells. Peak features may be due to resonant excitations followed by double autoionizations. The latter contributions are relatively small for W$^{5+}$ and were not considered in the theoretical cross-section calculations.

The present experimental absolute cross sections and the fine-step energy scan are compared to theoretical single-ionization cross sections for the two levels of the ground configuration in Fig. 3. The calculated cross sections for ionization from the lower and upper levels of the $5d$ ground configuration (levels 0 and 1, respectively, in Table I) are very similar to one another, with the cross section for the $5d\,^2D_{5/2}$ excited level slightly higher than that of the $5d\,^2D_{3/2}$ ground level. Theoretical cross sections corresponding to excitations to shells with principal quantum numbers up to $n = 7$ and $n = 12$, respectively, are shown for comparison. It can be seen that there is a difference of $\sim$20% between the $n = 7$ and the $n = 12$ result at the peak of the cross section. Previous studies for much more highly charged tungsten ions W$^{18+}$

TABLE I. Long-lived levels of the W$^{5+}$ ion and the associated lifetimes. Only levels with lifetimes exceeding $10^{-5}$ s are presented. Note that $a \pm b \equiv a \times 10^{\pm b}$.

| Configuration | Index | Level | $J$ | Energy (eV) | Lifetime (s) |
|---|---|---|---|---|---|
| $5d$ | 0 | $5d_-$ | 3/2 | 0 | – |
| | 1 | $5d_+$ | 5/2 | 1.122 | 1.25−1 |
| $6s$ | 2 | $6s_+$ | 1/2 | 9.681 | 3.15−4 |
| $4f^{13}5d^2$ | 6 | $4f^7_+\,5d^2_-\,(2)$ | 11/2 | 32.624 | 6.08+3 |
| | 7 | $4f^7_+\,5d^2_-\,(2)$ | 9/2 | 32.787 | 1.49+0 |
| | 8 | $4f^7_+\,5d_-\,2\,5d_+$ | 9/2 | 33.294 | 1.13−1 |
| | 10 | $4f^7_+\,5d_-\,5\,5d_+$ | 13/2 | 33.479 | 1.21−1 |
| | 14 | $4f^7_+\,5d_-\,3\,5d_+$ | 11/2 | 33.728 | 9.14−2 |
| | 16 | $4f^7_+\,5d_-\,5\,5d_+$ | 15/2 | 34.111 | 4.37−1 |
| | 17 | $4f^7_+\,5d_-\,5\,5d_+$ | 9/2 | 34.225 | 4.30−2 |
| | 19 | $4f^7_+\,5d_-\,5\,5d_+$ | 11/2 | 34.448 | 1.27−1 |
| | 22 | $4f^7_+\,5d^2_+\,(4)$ | 13/2 | 34.519 | 1.73−1 |
| | 26 | $4f^5_-\,5d^2_-\,(2)$ | 9/2 | 34.919 | 1.25−2 |
| | 27 | $4f^7_+\,5d_-\,3\,5d_+$ | 9/2 | 34.985 | 5.47−2 |
| | 31 | $4f^7_+\,5d^2_+\,(4)$ | 15/2 | 35.345 | 5.00−2 |
| | 32 | $4f^7_+\,5d_-\,4\,5d_+$ | 11/2 | 35.368 | 3.18−2 |
| | 35 | $4f^7_+\,5d_-\,4\,5d_+$ | 9/2 | 35.374 | 3.95−2 |
| | 40 | $4f^5_-\,5d_-\,4\,5d_+$ | 11/2 | 35.945 | 8.63−3 |
| | 41 | $4f^7_+\,5d^2_+\,(2)$ | 9/2 | 35.992 | 2.82−2 |
| | 44 | $4f^5_-\,5d_-\,2\,5d_+$ | 9/2 | 36.274 | 9.19−3 |
| | 45 | $4f^7_+\,5d^2_+\,(2)$ | 11/2 | 36.282 | 3.54−2 |
| | 47 | $4f^7_+\,5d^2_+\,(4)$ | 13/2 | 36.424 | 2.08−2 |
| | 51 | $4f^5_-\,5d_-\,4\,5d_+$ | 13/2 | 36.735 | 1.07−2 |
| | 53 | $4f^5_-\,5d_-\,2\,5d_+$ | 9/2 | 36.799 | 1.52−2 |
| | 56 | $4f^7_+\,5d^2_+\,(4)$ | 9/2 | 36.973 | 1.51−2 |
| | 59 | $4f^7_+\,5d^2_+\,(2)$ | 11/2 | 37.226 | 1.38−2 |
| | 62 | $4f^5_-\,5d^2_+\,(4)$ | 11/2 | 37.345 | 1.11−2 |
| | 64 | $4f^5_-\,5d^2_+\,(4)$ | 9/2 | 37.762 | 6.77−3 |
| | 68 | $4f^5_-\,5d^2_+\,(4)$ | 13/2 | 38.022 | 6.78−3 |
| | 75 | $4f^5_-\,5d^2_+\,(2)$ | 9/2 | 38.912 | 7.03−3 |
| | 79 | $4f^5_-\,5d^2_+\,(4)$ | 11/2 | 39.166 | 6.91−3 |
| | 81 | $4f^5_-\,5d^2_+\,(4)$ | 9/2 | 39.552 | 6.98−3 |
| $5p^55d^2$ | 87 | $5p^3_+\,5d_-\,1\,5d_+$ | 7/2 | 38.134 | 7.30−5 |
| | 89 | $5p^3_+\,5d_-\,2\,5d_+$ | 9/2 | 38.712 | 1.49−1 |
| | 91 | $5p^3_+\,5d^2_+\,(4)$ | 11/2 | 39.034 | 3.58−1 |
| | 98 | $5p^3_+\,5d^2_+\,(4)$ | 9/2 | 40.760 | 1.13−2 |
| | 99 | $5p^3_+\,5d_-\,3\,5d_+$ | 11/2 | 41.002 | 4.76−2 |
| | 105 | $5p^3_+\,5d_-\,2\,5d_+$ | 9/2 | 42.641 | 1.66−2 |
| | 116 | $5p_-\,5d_-\,2\,5d_+$ | 9/2 | 51.551 | 6.68−5 |
| | 121 | $5p_-\,5d^2_+\,(4)$ | 9/2 | 53.355 | 6.57−5 |
| $4f^{13}5d\,6s$ | 129 | $4f^7_+\,5d_-\,2\,6s_+$ | 5/2 | 43.657 | 2.07−4 |
| | 131 | $4f^7_+\,5d_-\,5\,6s_+$ | 9/2 | 44.397 | 2.02−4 |
| | 132 | $4f^7_+\,5d_-\,5\,6s_+$ | 11/2 | 44.583 | 1.73−4 |
| | 133 | $4f^7_+\,5d_-\,3\,6s_+$ | 7/2 | 44.859 | 1.66−4 |
| | 134 | $4f^7_+\,5d_-\,3\,6s_+$ | 5/2 | 45.085 | 1.73−4 |
| | 135 | $4f^7_+\,5d_-\,4\,6s_+$ | 9/2 | 45.261 | 1.54−4 |
| | 136 | $4f^7_+\,5d_-\,4\,6s_+$ | 7/2 | 45.315 | 1.68−4 |
| | 137 | $4f^7_+\,5d_+\,6\,6s_+$ | 13/2 | 45.361 | 1.70−4 |

TABLE I. (*Continued.*)

| Configuration Index | Level | $J$ | Energy (eV) | Lifetime (s) |
|---|---|---|---|---|
| 140 | $4f_+^7\,5d_+\,2\,6s_+$ | 5/2 | 46.018 | 1.62−4 |
| 142 | $4f_+^7\,5d_+\,6\,6s_+$ | 11/2 | 46.246 | 1.45−4 |
| 143 | $4f_+^7\,5d_+\,4\,6s_+$ | 9/2 | 46.258 | 1.56−4 |
| 144 | $4f_+^7\,5d_+\,3\,6s_+$ | 7/2 | 46.263 | 1.64−4 |
| 145 | $4f_+^7\,5d_+\,5\,6s_+$ | 11/2 | 46.583 | 1.30−4 |
| 146 | $4f_-^5\,5d_-\,4\,6s_+$ | 7/2 | 46.683 | 1.79−4 |
| 147 | $4f_+^7\,5d_+\,3\,6s_+$ | 5/2 | 47.001 | 1.32−4 |
| 148 | $4f_-^5\,5d_-\,4\,6s_+$ | 9/2 | 47.034 | 1.73−4 |
| 150 | $4f_-^5\,5d_-\,2\,6s_+$ | 5/2 | 47.231 | 1.78−4 |
| 151 | $4f_+^7\,5d_+\,4\,6s_+$ | 7/2 | 47.269 | 1.30−4 |
| 153 | $4f_+^7\,5d_+\,5\,6s_+$ | 9/2 | 47.455 | 1.30−4 |
| 154 | $4f_-^5\,5d_-\,3\,6s_+$ | 5/2 | 47.781 | 1.49−4 |
| 156 | $4f_-^5\,5d_-\,3\,6s_+$ | 7/2 | 47.945 | 1.59−4 |
| 158 | $4f_-^5\,5d_+\,5\,6s_+$ | 11/2 | 48.060 | 1.73−4 |
| 159 | $4f_-^5\,5d_-\,2\,6s_+$ | 5/2 | 48.377 | 1.56−4 |
| 160 | $4f_-^5\,5d_+\,3\,6s_+$ | 7/2 | 48.713 | 1.52−4 |
| 161 | $4f_-^5\,5d_+\,4\,6s_+$ | 9/2 | 48.727 | 1.41−4 |
| 163 | $4f_-^5\,5d_+\,5\,6s_+$ | 9/2 | 49.089 | 1.36−4 |
| 165 | $4f_-^5\,5d_+\,3\,6s_+$ | 5/2 | 49.605 | 1.27−4 |
| 167 | $4f_-^5\,5d_+\,4\,6s_+$ | 7/2 | 49.851 | 1.29−4 |

[52], $W^{25+}$ [53], $W^{26+}$ [54], and $W^{27+}$ [55,56] demonstrated the importance of excitations to higher shells ($n > 12$) which were needed to reach convergence of the EA cross sections while contributions with $n > 12$ were found to be negligible for the ionization of $W^{5+}$. The deeper reason for the different levels of importance of high-$n$ contributions to the ionization cross sections of $W^{5+}$ and $W^{q+}$ with $q \geqslant 18$ is not known. The effect is probably associated with the very different charge states and the resulting different electronic structures of those ions.

Comparisons of theory and experiment similar to the one in Fig. 3 have been presented previously [21,24,25]. The calculations were restricted to the ground configuration and ground level, respectively. In spite of this restriction, the agreement with the experimental cross section at energies beyond about 70 eV was interpreted although the experimental data are not for the ground level or ground configuration but for a mixture of ions in the ground state and in metastable levels. The pioneering CADW calculations by Pindzola and Griffin [21] with excitations up to shells with $n = 7$ and orbital quantum numbers $l = 4$ for indirect ionization processes showed very good agreement with the measurements reported by Stenke *et al.* [2] at energies beyond the ground-state ionization potential. These data are slightly below our results for the $n \leqslant 7$ case. It should be noted that our study includes also excitations to shells with $l = 5$ and $l = 6$ but their contribution is negligible. It is known that the CADW approach can lead to inaccurate probabilities of Auger transitions for overlapping initial and final configurations [57,58]. Moreover, the pseudorelativistic approach has been used by Pindzola and Griffin to obtain wave functions for the structure and scattering calculations while our calculations employ the Dirac-Fock-Slater method.
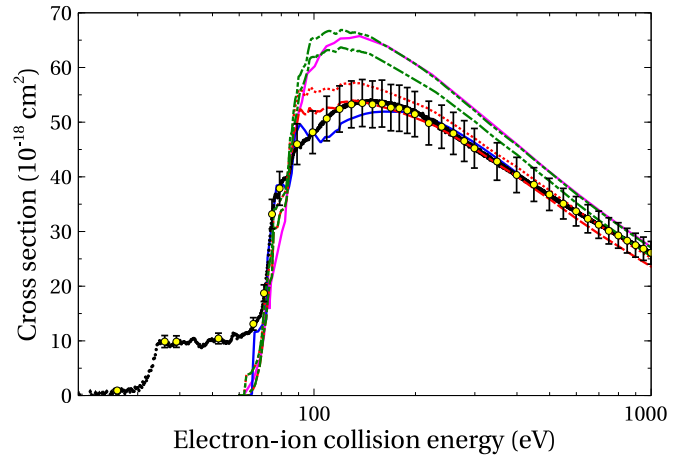


FIG. 3. Comparison of the present experimental data to the theoretical calculations for single ionization from the ground levels of $W^{5+}$. Circles with light shading (yellow) and associated total error bars represent experimental absolute cross sections. The small black dots with statistical error bars of the size of the symbols are the result of the fine-step energy scan. Present theoretical results including DI and EA for excitations with $n \leqslant 7$ are shown by the dashed (red) line for the $5d\,^2D_{3/2}$ ground level and by the dotted (red) line for the $5d\,^2D_{5/2}$ level. The dash-dotted (green) line represents the $5d\,^2D_{3/2}$ cross section and the dash-dot-dotted (green) line the $5d\,^2D_{5/2}$ cross section which both contain EA contributions associated with excitations up to $n = 12$. The upper solid (magenta) line represents the calculation performed by Zhang *et al.* [25] that includes EA contributions up to $n = 10$. The CADW results obtained by Pindzola and Griffin [21] including excitations with $n \leqslant 6$ are represented by the solid (blue) line that is close to the experimental data points.

Furthermore, our study includes radiative damping of the autoionizing states. This leads to diminishing of the total ionization cross sections by $\sim 14\%$ at the peak. Instead, the previous CADW treatment found that the branching ratio for autoionization is approximately equal to one [21].

In Fig. 3 we also compare our data with the recent LLDW calculations by Zhang *et al.* [25]. The minor deviations of the results of Zhang *et al.* from our theoretical cross section can be explained by slight differences between both theoretical approaches. In their calculations of EA cross sections, Zhang *et al.* [25] considered excitations into levels with $n \leqslant 10$. In the present work, slightly higher principal quantum numbers of up to $n = 12$ are taken into account, in addition. The treatment of DI cross sections differs in that Zhang *et al.* optimized their continuum wave functions on the primary ion while, here, we used the potential of the product-ion.

The contribution $\delta_{11}$ of the EA channels to the $W^{5+}$ ionization cross section comprising excitations to the shell with the principal quantum number $n = 11$ is $\delta_{11} \approx 1.1$ Mb at the peak of the cross section while the shell with $n = 12$ adds only $\delta_{12} \approx 0.8$ Mb. Assuming that the ratio of the contributions of shell $n + 1$ and shell $n$ is equal to $\delta_{n+1}/\delta_n = 0.8/1.1 = 0.723$ for all $n \geqslant 12$ we obtain a geometrical series of cross-section contributions $\sum_{n=12}^{\infty} \delta_n = \delta_{12} \sum_{\nu=0}^{\infty} 0.723^\nu$ from which we may estimate that the excitations to the higher shells ($n > 12$) provide less than 5% to the total cross section. However, our
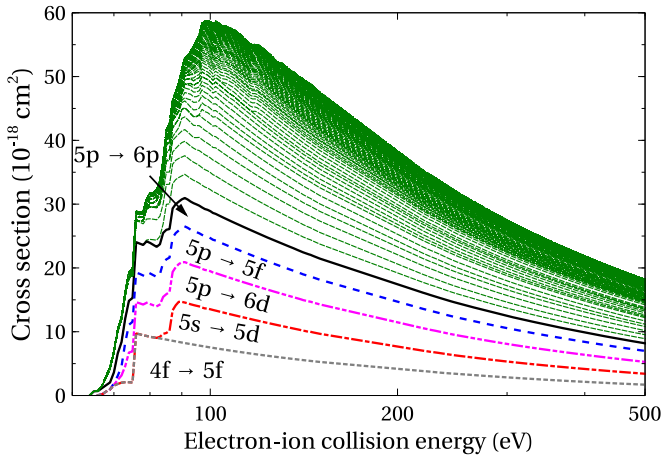
FIG. 4. Accumulated cross sections of the EA channels contributing to the ionization of the ground level of W$^{5+}$. The strongest EA contributions are individually identified.



FIG. 5. Accumulated electron-impact single-ionization cross sections for ground-level W$^{5+}$. The shaded areas show contributions of DI processes from different subshells.

study does not include events where the outgoing electron removes an additional electron from the ion, thereby leading to double ionization [59]. Additional emission of a bound electron has a diminishing effect on the theoretical single-ionization cross sections (as studied for the Se$^{3+}$ ion [60]). However, this effect is expected to involve less than 5% of the single-ionization cross sections since double-ionization cross sections are $\approx$3 Mb [6] at the peak compared to $\approx$60 Mb for the single ionization.

The ionization onset of the experimental cross section (see Fig. 2) at about 30 eV, i.e., approximately 35 eV below the ground-state ionization threshold, suggests that a fraction of ions in metastable states was present in the ion beam used for the measurements. The flight time of ions from the ion source to the interaction region equaled $\approx$1.5 $\times$ 10$^{-5}$ s. Hence, excited ions produced in the ion source must have lifetimes which exceed this value to be able to reach the interaction region. The long-lived levels with index $i$ filtered in such a way are listed in Table I together with their corresponding lifetimes $\tau_i$ calculated in the single-configuration approach (the level indices given in the Table I are used throughout the text).

There are 29 levels which belong to the $4f^{13}5d^2$ configuration, 8 levels from the $5p^55d^2$ configuration, and 28 levels of $4f^{13}5d\,6s$ configuration with sufficiently long lifetimes. These were calculated with consideration of electric dipole, quadrupole, and octupole, as well as magnetic dipole and quadrupole transitions from the levels of the $5d$, $6s$, $4f^{13}5d^2$, $5p^55d^2$, and $4f^{13}5d\,6s$ configurations. The lowest excited configuration of the W$^{5+}$ ion involves a $5d \rightarrow 6s$ promotion from the ground configuration. The configuration can decay via very weak electric quadrupole transitions. Many levels of the other three configurations decay via electric dipole transitions. However, selection rules for the electric dipole transitions limit the possible decay paths for some levels. Such levels feature long lifetimes.

The cross sections of the strongest EA channels for the ground level of W$^{5+}$ are shown in Fig. 4. Five transitions ($4f \rightarrow 5f$, $5s \rightarrow 5d$, $5p \rightarrow 6d$, $5p \rightarrow 5f$, $5p \rightarrow 6p$) produce approximately half of the total EA cross sections.
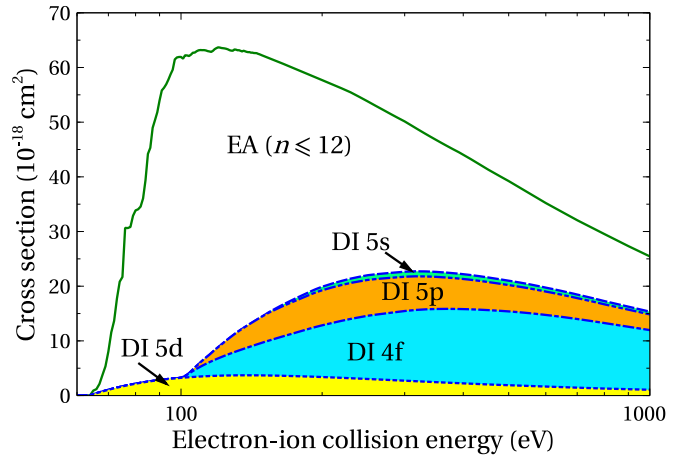
Only one ($5p \rightarrow 6d$) of the presented excitations leads to an odd-parity configuration. All the final configurations of the strongest excitations have energy levels above the single-ionization threshold with the exception of the $5p^55d\,6p$ configuration whose levels are partly below that threshold (Fig. 1).

The contributions of direct and indirect processes of ionization by electron impact from the ground configuration are shown in Fig. 5. The strongest DI contribution is associated with ionization of the $4f$ subshell which has the largest number of electrons. Indirect processes dominate over DI at the lower electron energies. It should be noted that EA dominates over DI particularly for the excited initial configurations. The largest EA contribution originates from the $5p \rightarrow 5d$ promotion. This is true for all the considered initial configurations except the $5d$ configuration. The reason for this exception becomes obvious when one looks at Fig. 1: All levels of the excited $5p^55d^2$ configuration are lower than the ionization threshold. The $5p \rightarrow 5d$ excitation cross sections are much larger than the DI cross sections which are very similar for all presented configurations. This confirms the expectations expressed previously by Stenke *et al.* (see Sec. I).

We note that all theoretical single-configuration cross sections are well above the measurements. It is a well-known fact that the DW approximation overestimates cross sections for neutral atoms and near-neutral ions. Therefore, Kim and associates introduced the "scaled plane-wave Born" (PWB) method to determine cross sections that are in better agreement with measurements [61,62]. It was suggested that the proposed scaling mimics the effects related to electron exchange, distortion and polarization that are missing in the first order PWB approximation. The binary-encounter-dipole and binary-encounter-Bethe (BEB) models were subsequently developed for DI processes [63]. A similar approach was applied to DW cross-section calculations in the analysis of ionization of the carbon atom and the C$^{1+}$ ion [64]. Unfortunately, the method of scaled DW cross sections does not reproduce the experimental values for the W$^{5+}$ ion. This demonstrates that other physical effects are responsible for the formation of the W$^{6+}$ ions in the ionization process of W$^{5+}$.
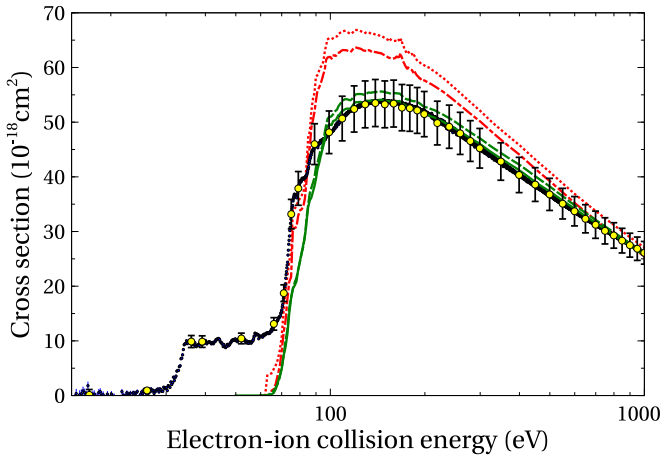
FIG. 6. Comparison of electron-impact ionization cross sections for W$^{5+}$ obtained in the single-configuration approximation (upper pair of red lines) and by using a basis of interacting configurations (lower pair of green lines). The solid (green) and the long-dash-short-dashed (red) lines represent the cross sections of the $5d\ ^2D_{3/2}$ ground level. The long-dashed (green) and the dotted (red) lines represent the cross section of the $5d\ ^2D_{5/2}$ excited level. For further details see the main text.

The influence of correlation effects on direct and indirect processes of ionization has been studied for the $5d$ configuration using the configuration-interaction (CI) method. A list of admixed configurations having the largest effect for the considered configuration was generated using the CIS concept [see Eq. (3)]. The same approach was applied previously to electric [65] and magnetic dipole transitions [66,67], Auger cascades [68–70], and electron-impact ionization [71,72]. For excitations to levels with the same parity as the initial level, the basis of interacting configurations has to include the initial configuration. It is found that CI has a crucial effect on the results.

A comparison of cross sections obtained in the single-configuration approximation and by using the CI method is presented in Fig. 6. It can be seen that correlation effects diminish the cross sections by $\approx 20\%$ at the maximum. The CI cross sections are within the error bars of the experimental cross sections at the maximum and at higher energies. However, as mentioned in the context of Fig. 3 this agreement with the experiment is meaningless as long as the contributions of metastable parent ions are not included. The purpose of the present comparison is to show that two counteracting effects have produced the agreement of the cross sections calculated by Pindzola and Griffin with the experiments. Their treatment included only excitations to shells with $n \leqslant 7$ (Fig. 3) and did not account for CI effects while the present calculations include excitations up to $n = 12$ and take CI into account. We note that the largest effect in the CI study is obtained for the $4f \rightarrow 5f$ excitation. The CI effects reduce the associated cross sections by $\approx 8$ Mb (corresponding to $\approx 80\%$) around the maximum.

To reproduce the experimental cross section and to test the validity of the theoretical approaches it is necessary to consider not only the ground state of the W$^{5+}$ ion but also all possible (long-lived) excited levels of W$^{5+}$ ions that have been
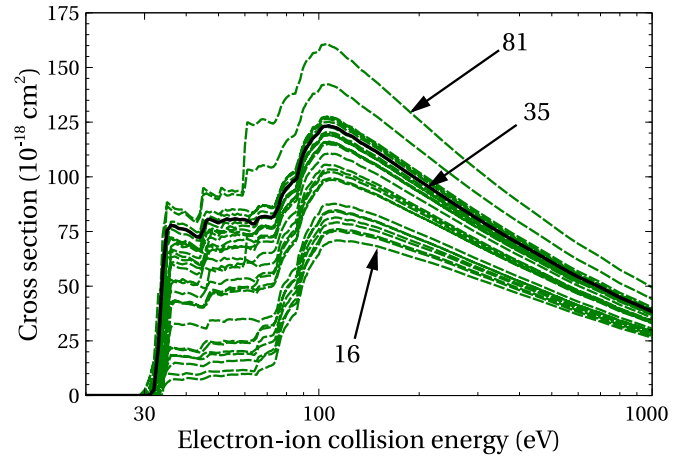


FIG. 7. Cross sections for the long-lived levels (as listed in Table I) of the $4f^{13}5d^2$ configuration. Few selected cross-section functions are labeled by their index given in Table I. The excitation function of the level with index 35 (see text) is shown by the solid black line.

present in the parent ion beam used during the measurements. The levels which have to be taken into account are listed in Table I. Total single-ionization cross sections including the DI and EA contributions have been calculated for each level listed in the table. For the excited configurations the inclusion of CI effects would have made the calculations too large. Therefore, CI was only taken into account for the ground configuration. Examples for cross sections are presented in Figs. 7 and 8 for the levels associated with the $4f^{13}5d^2$ and $5p^55d^2$ configurations, respectively, as listed in Table I. One can note a very strong dependence of the data on the level for which the ionization process is studied. The same situation was obtained for the electron-impact ionization from levels of the W$^{26+}$ ion [73]. This demonstrates the decisive importance of level-to-level calculations for the ionization of the W$^{5+}$ ion.
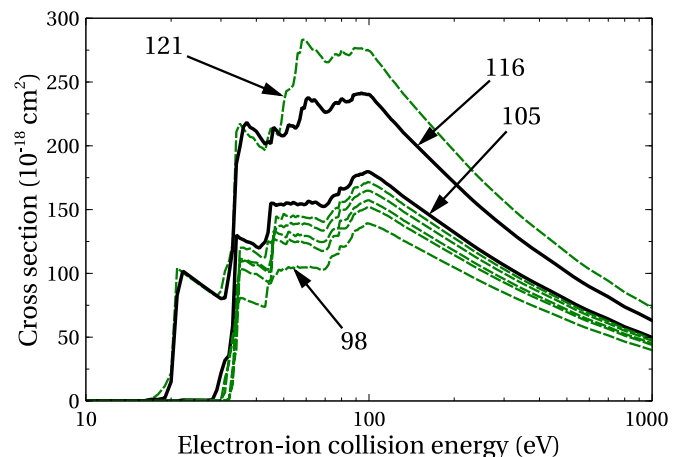


FIG. 8. Cross sections for the long-lived levels (as listed in Table I) of the $5p^55d^2$ configuration. Few selected cross-section functions are labeled by their index given in Table I. The excitation function of the levels with indices 105 and 116 (see text) are shown by solid black lines.

## C. Theoretical modeling of metastable fraction

For the comparison of the calculated cross sections with the experimental results shown in Fig. 2 it is necessary to know the fractions $\lambda_i$ of ions in all possible levels (index $i$, see Table I) that contributed to the measured single-ionization spectrum [see Eq. (5)]. These fractions are not *a priori* known from the experiment. This problem has been addressed previously in the context of storage-ring electron-ion recombination measurements with tungsten ions [74,75]. In these investigations, the temporal evolutions of level populations were calculated assuming the population of excited levels with a Maxwell distribution when the fast parent ions pass a stripper foil and then using rate equations to describe the radiative decays of these levels [76] until the ions interact with the target electrons. The time span for the ions to relax in these experiments was of the order of seconds, quite different from the $\approx$15 microsecond time-of-flight in the present experiment for which three different approaches have been applied to assess all $\lambda_i$ and to model the experimental data thereby on the basis of the calculated cross sections.

Since the W$^{5+}$ ions are produced in the ion source plasma it makes sense to assume statistical populations of levels within each of the contributing configurations, in the present case $5d$, $6s$, $4f^{13}5d^2$, $5p^55d^2$, and $4f^{13}5d\,6s$. This kind of assumption has been successfully applied in numerous previous studies of collision processes involving ion beams and is considered to be the most realistic approach also to the present problem. With this starting condition Eq. (5) is modified to

$$\sigma^{\exp}(E_e) = \sum_k c_k \frac{\sum_i (2 \times {}^kJ_i + 1) \times {}^k\sigma_i^{\mathrm{th}}(E_e)}{\sum_i (2 \times {}^kJ_i + 1)}, \qquad (6)$$

where $c_k$ are fitting parameters for each of the five configurations considered (see Table I), the fraction with a sum over $i$ in the numerator and in the denominator is the configuration averaged cross section for the long-lived levels $i$ in configuration $k$, ${}^kJ_i$ is the total angular momentum quantum number of level $i$ in configuration $k$ and ${}^k\sigma_i^{\mathrm{th}}(E_e)$ is the total single-ionization cross section for level $i$ in configuration $k$.

The analysis of an experiment, in which the cross section for photoionization of W$^{5+}$ was measured and for which relativistic R-matrix calculations were performed, suggests that the ECR ion source employed in both experiments produced 2.5% of ions in the metastable $6s$ configuration [77]. This knowledge reduces the number of free fitting parameters $c_k$ to four. The remaining fitting parameters in this model, apart from $c_2 = 0.025$ for the $6s$ configuration were determined to be $c_1 = 0.85$ for the $5d$ ground configuration, $c_3 = 0.082$ for $4f^{13}5d^2$, $c_4 = 0.036$ for $5p^55d^2$, and $c_5 = 0.007$ for $4f^{13}5d\,6s$. The energy range from 20 to 80 eV was used to determine the best agreement of the theoretical models with the measurements. It is noted that a fit over a wider energy range leads to lower cross sections for the contribution of metastable ions at energies below the ground-state ionization threshold. This corresponds to the lower metastable fraction of the ion beam in the theoretical model. Therefore, the highest limit for the metastable fraction is approximately determined using the energy range of 20–80 eV in the modeling. The theoretical model cross section resulting from the fit over the 20 to 80 eV range is represented by the green solid line in
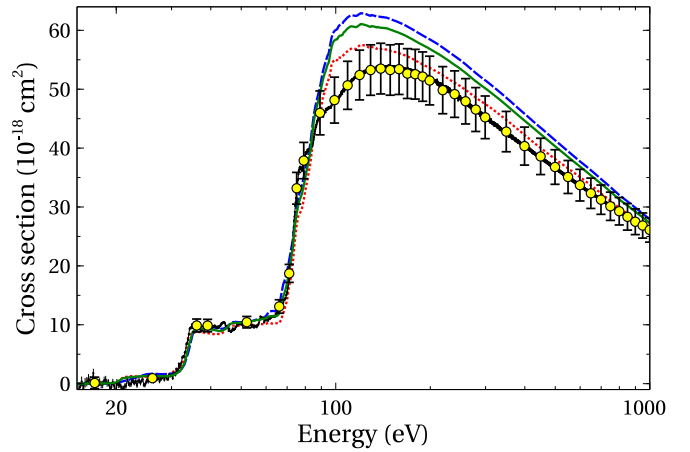


FIG. 9. Electron-impact ionization cross sections for the W$^{5+}$ ion. Circles with error bars and (yellow) shading: experimental absolute cross sections, solid black noisy line: fine-step energy-scan data. The (green) solid line is the result of model 1 [see Eq. (6) and text], the dashed (blue) line corresponds to model 2 [see Eq. (7) and text]. The dotted (red) line is obtained from model 3 [see Eqs. (5), (8) and text].

Figs. 9 and 10. This line is in very good agreement with the cross section below the ground-state ionization threshold. It is slightly above the experimental cross section particularly at energies around 100 eV. Correlation effects not considered for the ionization from the excited configurations can be a reason of the disagreement. It may also be due to the model chosen for reproducing the experimental cross section.

A second model reduces the number of fitting parameters to one. With the argument that the ions are primarily produced in a plasma one may assume a Boltzmann distribution for the population of excited levels. This reduces the problem to fitting the temperature $T$. Equation (5) then takes the form

$$\sigma^{\exp}(E_e) = \frac{\sum_{i=1}^m (2J_i + 1)\exp[-E_i/(kT)]\sigma_i^{\mathrm{th}}(E_e)}{\sum_{i=1}^m (2J_i + 1)\exp[-E_i/(kT)]}. \qquad (7)$$
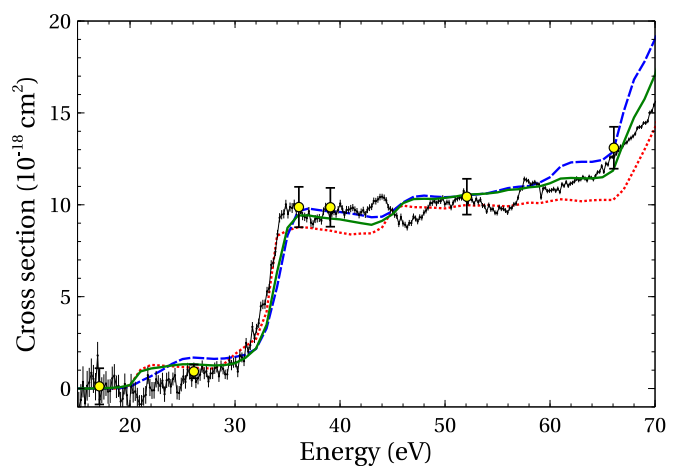


FIG. 10. Same as Fig. 9 in the energy range where only metastable levels contribute to the total single-ionization cross section.

TABLE II. Fractions of ions in different initial configurations present in the parent ion beam that was used in the experiments. The numbers obtained depend on the model assumptions (see main text).

| model | $5d$ | $6s$ | $4f^{13}5d^2$ | $5p^55d^2$ | $4f^{13}5d6s$ |
|---|---|---|---|---|---|
| 1 | 0.85 | 0.025 | 0.082 | 0.036 | 0.007 |
| 2 | 0.788 | 0.041 | 0.137 | 0.014 | 0.020 |
| 3 | 0.935 | 0 | 0.012 | 0.053 | 0 |

Here, $J_i$ is the total angular momentum quantum number and $E_i$ the excitation energy of level $i$. A temperature $T = 78\,000$ K brings this model into the best agreement with the experiment. This is within the temperature range predicted for producing moderately low charge states of tungsten ions such as $W^{4+}$ and $W^{5+}$ in a coronal-equilibrium plasma [78].

The model cross section shown in Fig. 10 as a long-dashed (blue) line describes the measured data below the ground-state ionization threshold very well. At energies above approximately 100 eV it is even higher than the cross section resulting from the first model, however, the difference is relatively small. The corresponding fractions of ions in the relevant configurations are 78.8% for the $5d$ configuration, 4.1% for $6s$, 13.7% for $4f^{13}5d^2$, 1.4% for $5p^55d^2$, and 2.0% for $4f^{13}5d\,6s$. With 4.1% the $6s$ fraction is overestimated in comparison with the photoionization experiment where 2.5% have been found. The maximum deviation of the Boltzmann model from the experiment is about 20% near 100 eV. It is about 10% above the experimental error bars.

The third model treats all 68 fractions $\lambda_i$ in Eq. (5) as free fitting parameters. Since the measured electron-impact ionization cross sections obtained in the present energy scan comprise more than 5000 data points with a very specific energy dependence such a fit with that many parameters is less ambiguous than one might think. However, the model is rooted more in mathematical methods than in the physics of ion sources and ion beams. The fractions $\lambda_i$ are chosen such that the function

$$f(\lambda_1, \lambda_2, \ldots, \lambda_m) = \left[ \sigma^{\exp}(E_e) - \sum_{i=1}^{m} \lambda_i \sigma_i^{\text{th}}(E_e) \right]^2. \quad (8)$$

reaches a minimum.

The minimum is obtained when only four levels are assumed to contribute to the sum in Eq. (8), the ground level with $\approx 93.5\%$, the level with index 35 belonging to the $4f^{13}5d^2$ configuration contributing 1.2% and two levels of the $5p^55d^2$ configuration with indices 105 and 116 contributing 4.1% and 1.2%, respectively. While this model is more speculative, and probably the least physical of the three, it gives the best agreement with the measured cross-section function. However, it is highly doubtful that only 4 levels out of 68 should be present in the ion beam. All the three models give a very good representation of the cross-section contributions observed in the experiment below the ground-state ionization threshold as emphasized in Fig. 10. The comparison of the three models in Table II elucidates the uncertainty of the fractions of ions in different levels that contributed to the measured cross section. The fraction of ions in the ground configuration is most likely $c_1 = 0.85$ for which a 10%

relative-uncertainty margin seems realistic. Accordingly, the metastable fractions derived from the comparisons of theory and experiment have very substantial relative uncertainties.

## V. CONCLUSIONS

We report absolute experimental electron-impact single-ionization cross sections for $W^{5+}$ and a detailed scan of the cross section as a function of electron energy together with a thorough theoretical study employing the distorted-wave approximation to both direct-ionization and to excitation-autoionization contributions of the cross section. The present experimental results are in good agreement with previously published experimental data. The measured energy scan revealed nonzero ionization signal below the ionization threshold of the ground level clearly indicating the presence of ions in excited long-lived states in the ion beam employed in the experiments.

To understand the measured cross-section function, level-to-level calculations were carried out for the relevant five initial configurations with consideration of the effects of configuration interaction. Radiative damping is explicitly taken into account in the calculations and reduces the cross sections depending on the levels considered. It is shown that correlation effects play a crucial role in explaining the experimental data. Correlation effects reduce the theoretical cross sections obtained for the ground configuration by $\approx 20\%$. On the basis of the theoretical cross sections which were calculated for both levels of the ground configuration and for the long-lived levels of the $6s$, $4f^{13}5d^2$, $5p^55d^2$, and $4f^{13}5d\,6s$ configurations, the experimental cross-section function could be reproduced reasonably well. Three models were used to determine the fractions of $W^{5+}$ ions in different electronic levels present in the parent-ion beam. With the theoretical cross sections for the excited configurations listed above which had not been assessed previously, the cross sections observed in the experiment below the ground-state ionization threshold are reproduced extremely well when energy range from 20 to 80 eV is used in the modeling. Even a small cross section contribution in the 20–30 eV region observed in the experiment is reproduced by our theoretical results in all three models. Around the maximum, all theoretical-model cross sections are slightly too high. The disagreement among theoretical and experimental values can be related to the correlation effects that are not accounted in the calculations of configuration interactions for the excited configurations due to limitations in the computing resources.

Strong $5p \rightarrow 5d$ and $4f \rightarrow 5d$ excitations from the ground configuration were found in the present calculations suggesting that these excitations could be responsible for the electron-impact excitation of $W^{5+}$ metastable states in the ion source. The ions are effectively trapped for some time in the space-charge field of the electrons in the ion-source plasma. Then they spend some time traveling in vacuum from the ion source to the interaction region. Thus, contributions of radiative cascades would have to be taken into account to analyze the population of the long-lived levels. The $6s$ configuration, for example, might be populated by $5d \rightarrow 6p$, $5d \rightarrow 6d$, and $5d \rightarrow 6f$ excitations from the ground configuration with subsequent radiative cascades. For a more accurate assessment

of the population distribution of ions in the parent ion beam collisional radiative modeling of the processes in the ion source and subsequent radiative decay during the flight of the ions to the interaction region may be needed to estimate the population of levels in such measurements [47].

[1] R. G. Montague and M. F. A. Harrison, J. Phys. B: At. Mol. Opt. Phys. **17**, 2707 (1984).

[2] M. Stenke, K. Aichele, D. Harthiramani, G. Hofmann, M. Steidl, R. Völpel, and E. Salzborn, J. Phys. B: At. Mol. Opt. Phys. **28**, 2711 (1995).

[3] J. Rausch, A. Becker, K. Spruck, J. Hellhund, A. Borovik Jr., K. Huber, S. Schippers, and A. Müller, J. Phys. B: At. Mol. Opt. Phys. **44**, 165202 (2011).

[4] A. Borovik Jr., B. Ebinger, D. Schury, S. Schippers, and A. Müller, Phys. Rev. A **93**, 012708 (2016).

[5] D. Schury, A. Borovik Jr., B. Ebinger, F. Jin, K. Spruck, A. Müller, and S. Schippers, J. Phys. B: At. Mol. Opt. Phys. **53**, 015201 (2020).

[6] M. Stenke, K. Aichele, D. Harthiramani, G. Hofmann, M. Steidl, R. Völpel, V. P. Shevelko, H. Tawara, and E. Salzborn, J. Phys. B: At. Mol. Opt. Phys. **28**, 4853 (1995).

[7] W. Lotz, Z. Phys. **216**, 241 (1968).

[8] K. Aichele, U. Hartenfeller, D. Hathiramani, G. Hofmann, V. Schäfer, M. Steidl, M. Stenke, E. Salzborn, T. Pattard, and J.-M. Rost, J. Phys. B: At. Mol. Opt. Phys. **31**, 2369 (1998).

[9] J. M. Rost and T. Pattard, Phys. Rev. A **55**, R5 (1997).

[10] L. U. Ancarani and P.-A. Hervieux, Phys. Rev. A **72**, 034701 (2005).

[11] M. Szłuińska, P. Van Reeth, and G. Laricchia, J. Phys. B: At. Mol. Opt. Phys. **35**, 4059 (2002).

[12] I. Bray, D. V. Fursa, A. S. Kadyrov, A. Müller, A. Borovik, Jr., and S. Schippers, Phys. Rev. A **100**, 012707 (2019).

[13] M. A. de Avillez, M. Guerra, J. P. Santos, and D. Breitschwerdt, Astron. Astrophys. **631**, A42 (2019).

[14] J.-M. Rost and T. Pattard, J. Phys. B: At. Mol. Opt. Phys. **32**, L457 (1999).

[15] D. J. Yu, S. Rachafi, J. Jureta, and P. Defrance, J. Phys. B: At. Mol. Opt. Phys. **25**, 4593 (1992).

[16] C. Bélenger, D. S. Belić, D. J. Yu, and P. Defrance, J. Phys. B: At. Mol. Opt. Phys. **32**, 1097 (1999).

[17] K. Aichele, W. Arnold, H. Bräuning, D. Hathiramani, F. Scheuermann, R. Trassl, and E. Salzborn, Nucl. Instrum. Methods B **205**, 437 (2003).

[18] C. Bélenger, P. Defrance, E. Salzborn, V. P. Shevelko, H. Tawara, and D. B. Uskov, J. Phys. B: At. Mol. Opt. Phys. **30**, 2667 (1997).

[19] V. Fisher, Y. Ralchenko, A. Goldgirsh, D. Fisher, and Y. Maron, J. Phys. B: At. Mol. Opt. Phys. **28**, 3027 (1995).

[20] M. Hahn, A. Müller, and D. W. Savin, Astrophys. J. **850**, 122 (2017).

[21] M. S. Pindzola and D. C. Griffin, Phys. Rev. A **56**, 1654 (1997).

[22] S. D. Loch, J. A. Ludlow, M. S. Pindzola, A. D. Whiteford, and D. C. Griffin, Phys. Rev. A **72**, 052716 (2005).

[23] M. S. Pindzola, and D. C. Griffin, Phys. Rev. A **46**, 2486 (1992).

[24] A. V. Demura, M. B. Kadomtsev, V. S. Lisitsa, and V. A. Shurygin, JETP Lett. **101**, 85 (2015).

[25] D. Zhang, L. Xie, J. Jiang, Z. Wu, C. Dong, Y. Shi, and Y. Qu, Chin. Phys. B **27**, 053402 (2018).

[26] D.-H. Kwon, Y.-J. Rhee, and Y.-K. Kim, Int. J. Mass Spectrom. **252**, 213 (2006).

[27] L. Vainshtein, I. Beigman, Ph. Mertens, S. Brezinsek, A. Pospieszczyk, and D. Borodin, J. Phys. B: At. Mol. Opt. Phys. **44**, 125201 (2011).

[28] D.-H. Kwon, Y.-S. Cho, and Y.-O. Lee, Int. J. Mass Spectrom. **356**, 7 (2013).

[29] M. F. Gu, Can. J. Phys. **86**, 675 (2008).

[30] C. P. Ballance, S. D. Loch, M. S. Pindzola, and D. C. Griffin, J. Phys. B: At. Mol. Opt. Phys. **46**, 055202 (2011).

[31] A. Borovik, M. F. Gharaibeh, P. M. Hillenbrand, S. Schippers, and A. Müller, J. Phys. B: At. Mol. Opt. Phys. **46**, 175201 (2013).

[32] P. Defrance, F. Brouillard, W. Claeys, and G. Van Wassenhove, J. Phys. B: At. Mol. Opt. Phys. **14**, 103 (1981).

[33] A. Müller, K. Huber, K. Tinschert, R. Becker, and E. Salzborn, J. Phys. B: At. Mol. Opt. Phys. **18**, 2993 (1985).

[34] A. Müller, K. Tinschert, C. Achenbach, R. Becker, and E. Salzborn, Nucl. Instrum. Methods B **10**, 204 (1985).

[35] A. Müller, K. Tinschert, G. Hofmann, E. Salzborn, and G. H. Dunn, Phys. Rev. Lett. **61**, 70 (1988).

[36] A. Müller, G. Hofmann, K. Tinschert, and E. Salzborn, Phys. Rev. Lett. **61**, 1352 (1988).

[37] A. Müller, G. Hofmann, B. Weissbecker, M. Stenke, K. Tinschert, M. Wagner, and E. Salzborn, Phys. Rev. Lett. **63**, 758 (1989).

[38] J. Jacobi, H. Knopp, S. Schippers, A. Müller, S. D. Loch, M. Witthoeft, M. S. Pindzola, and C. P. Ballance, Phys. Rev. A **70**, 042717 (2004).

[39] J. Jacobi, H. Knopp, S. Schippers, W. Shi, and A. Müller, J. Phys. B: At. Mol. Opt. Phys. **38**, 2015 (2005).

[40] A. Borovik Jr., A. Müller, S. Schippers, I. Bray, and D. V. Fursa, J. Phys. B: At. Mol. Opt. Phys. **42**, 025203 (2009).

[41] F. Broetz, R. Trassl, R. W. McCullough, W. Arnold, and E. Salzborn, Phys. Scr. **2001**, 278 (2001).

[42] A. Müller, Atoms **3**, 120 (2015).

[43] R. Becker, A. Müller, C. Achenbach, K. Tinschert, and E. Salzborn, Nucl. Instrum. Methods B **9**, 385 (1985).

[44] J. Fricke, A. Müller, and E. Salzborn, Nucl. Instrum. Methods **175**, 379 (1980).

[45] K. Rinn, A. Müller, H. Eichenauer, and E. Salzborn, Rev. Sci. Instrum. **53**, 829 (1982).

[46] V. Jonauskas, S. Kučas, and R. Karazija, Lith. J. Phys. **49**, 415 (2009).

[47] A. Kynienė, S. Kučas, Š. Masys, and V. Jonauskas, Astron. Astrophys. **624**, A14 (2019).

[48] R. Karazija, *Introduction to the Theory of X-Ray and Electronic Spectra of Free Atoms* (Plenum Press, New York, 1996).

[49] R. Karazija and S. Kučas, J. Quant. Spectrosc. Radiat. Transf. **129**, 131 (2013).

[50] R. D. Cowan, *The Theory of Atomic Structure and Spectra* (University of California Press, Berkeley, CA, 1981).

[51] A. Kramida, Yu. Ralchenko, J. Reader, and NIST ASD Team, NIST Atomic Spectra Database (version 5.1) (National Institute of Standards and Technology, Gaithersburg, MD, 2013), http://physics.nist.gov/asd.

[52] D.-H. Zhang and D.-H. Kwon, J. Phys. B: At. Mol. Opt. Phys. **47**, 075202 (2014).

[53] A. Kynienė, S. Pakalka, Š. Masys, and V. Jonauskas, J. Phys. B: At. Mol. Opt. Phys. **49**, 185001 (2016).

[54] A. Kynienė, Š. Masys, and V. Jonauskas, Phys. Rev. A **91**, 062707 (2015).

[55] V. Jonauskas, A. Kynienė, G. Merkelis, G. Gaigalas, R. Kisielius, S. Kučas, Š. Masys, L. Radžiūtė, and P. Rynkun, Phys. Rev. A **91**, 012715 (2015).

[56] M. S. Pindzola, and S. D. Loch, Phys. Rev. A **93**, 062709 (2016).

[57] V. Jonauskas, R. Karazija, and S. Kučas, J. Electron. Spectros. Relat. Phenomena **107**, 147 (2000).

[58] V. Jonauskas, L. Partanen, S. Kučas, R. Karazija, M. Huttula, S. Aksela, and H. Aksela, J. Phys. B: At. Mol. Opt. Phys. **36**, 4403 (2003).

[59] V. Jonauskas, A. Prancikevičius, Š. Masys, and A. Kynienė, Phys. Rev. A **89**, 052714 (2014).

[60] S. Pakalka, S. Kučas, Š. Masys, A. Kynienė, A. Momkauskaitė, and V. Jonauskas, Phys. Rev. A **97**, 012708 (2018).

[61] Y.-K. Kim, Phys. Rev. A **64**, 032713 (2001).

[62] Y.-K. Kim and J.-P. Desclaux, Phys. Rev. A **66**, 012708 (2002).

[63] Y. K. Kim and M. E. Rudd, Phys. Rev. A **50**, 3954 (1994).

[64] V. Jonauskas, Astron. Astrophys. **620**, A188 (2018).

[65] A. Kynienė, V. Jonauskas, S. Kučas, and R. Karazija, Lith. J. Phys. **48**, 219 (2008).

[66] V. Jonauskas, R. Kisielius, A. Kynienė, S. Kučas, and P. H. Norrington, Phys. Rev. A **81**, 012506 (2010).

[67] V. Jonauskas, G. Gaigalas, and S. Kučas, At. Data Nucl. Data Tables **98**, 19 (2012).

[68] V. Jonauskas, R. Karazija, and S. Kučas, J. Phys. B: At. Mol. Opt. Phys. **41**, 215005 (2008).

[69] J. Palaudoux, P. Lablanquie, L. Andric, K. Ito, E. Shigemasa, J. H. D. Eland, V. Jonauskas, S. Kučas, R. Karazija, and F. Penent, Phys. Rev. A **82**, 043419 (2010).

[70] V. Jonauskas, S. Kučas, and R. Karazija, Phys. Rev. A **84**, 053415 (2011).

[71] J. Koncevičiūtė, S. Kučas, Š. Masys, A. Kynienė, and V. Jonauskas, Phys. Rev. A **97**, 012705 (2018).

[72] J. Koncevičiutė, S. Kučas, A. Kynienė, Š. Masys, and V. Jonauskas, J. Phys. B: At. Mol. Opt. Phys. **52**, 025203 (2019).

[73] A. Kynienė, G. Merkelis, A. Šukys, Š. Masys, S. Pakalka, R. Kisielius, and V. Jonauskas, J. Phys. B: At. Mol. Opt. Phys. **51**, 155202 (2018).

[74] K. Spruck, N. R. Badnell, C. Krantz, O. Novotný, A. Becker, D. Bernhardt, M. Grieser, M. Hahn, R. Repnow, D. W. Savin, A. Wolf, A. Müller, and S. Schippers, Phys. Rev. A **90**, 032715 (2014).

[75] N. R. Badnell, K. Spruck, C. Krantz, O. Novotný, A. Becker, D. Bernhardt, M. Grieser, M. Hahn, R. Repnow, D. W. Savin, A. Wolf, A. Müller, and S. Schippers, Phys. Rev. A **93**, 052703 (2016).

[76] M. Lestinsky, N. R. Badnell, D. Bernhardt, D. Bing, M. Grieser, M. Hahn, J. Hoffmann, B. Jordon-Thaden, C. Krantz, O. Novotný, D. A. Orlov, R. Repnow, A. Shornikov, A. Müller, S. Schippers, A. Wolf, and D. W. Savin, Astrophys. J. **758**, 40 (2012).

[77] A. Müller, S. Schippers, J. Hellhund, A. L. D. Kilcoyne, R. A. Phaneuf, and B. M. McLaughlin, J. Phys. B: At. Mol. Opt. Phys. **52**, 195005 (2019).

[78] S. P. Preval, N. R. Badnell, and M. G. O'Mullane, J. Phys. B: At. Mol. Opt. Phys. **52**, 025201 (2019).